BJ Cell

Biochem. J. (2012) **448**, 103–113 (Printed in Great Britain) doi:10.1042/BJ20120578

A novel dual-fluorescence strategy for functionally validating microRNA targets in 3′ untranslated regions: regulation of the inward rectifier potassium channel $K_{ir}2.1$ by miR-212

Dana GOLDONI[1], Janet M. YARHAM[1], Mary K. McGAHON, Anna O'CONNOR, Jasenka GUDURIC-FUCHS, Kevin EDGAR, Denise M. McDONALD, David A. SIMPSON and Anthony COLLINS[2]

Centre for Vision and Vascular Science, Queen's University of Belfast, Institute of Clinical Science, Block A, Royal Victoria Hospital, Grosvenor Road, Belfast, BT12 6BA, U.K.

Gene targeting by microRNAs is important in health and disease. We developed a functional assay for identifying microRNA targets and applied it to the K^+ channel $K_{ir}2.1$ [KCNJ2 (potassium inwardly-rectifying channel, subfamily J, member 2)] which is dysregulated in cardiac and vascular disorders. The 3′UTR (untranslated region) was inserted downstream of the mCherry red fluorescent protein coding sequence in a mammalian expression plasmid. MicroRNA sequences were inserted into the pSM30 expression vector which provides enhanced green fluorescent protein as an indicator of microRNA expression. HEK (human embryonic kidney)-293 cells were co-transfected with the mCherry-3′UTR plasmid and a pSM30-based plasmid with a microRNA insert. The principle of the assay is that functional targeting of the 3′UTR by the microRNA results in a decrease in the red/green fluorescence intensity ratio as determined by automated image analysis. The method was validated with miR-1, a known down-regulator of $K_{ir}2.1$ expression, and was used to investigate the targeting of the $K_{ir}2.1$ 3′UTR by miR-212. The red/green ratio was lower in miR-212-expressing cells compared with the non-targeting controls, an effect that was attenuated by mutating the predicted target site. miR-212 also reduced inward rectifier current and $K_{ir}2.1$ protein in HeLa cells. This novel assay has several advantages over traditional luciferase-based assays including larger sample size, amenability to time course studies and adaptability to high-throughput screening.

Key words: HeLa cell, HEK-293 cell, image analysis, microRNA, patch clamp.

INTRODUCTION

miRNAs (microRNAs) are increasingly recognised as important regulators of gene expression in health and disease. They exert their effects by interacting with target sequences in mRNA 3′ UTRs (untranslated regions) via a complementary 6–8 bp 5′ 'seed region' and variable imperfect complementarity in the rest of the ~22 nucleotide sequence [1]. This variability presents challenges for predicting miRNA target sites by bioinformatics. Available algorithms provide a good starting point for identifying potential miRNA target sites, but these predictions need to be tested with a functional assay before the sites can be identified unequivocally. Luciferase-based transfection assays are commonly used for this purpose, but these assays have limitations. We resolved to develop an improved approach based on a fluorescent reporter gene linked to a 3′UTR of interest, and pSM30, an expression vector that has a miRNA expression cassette in a synthetic intron of EGFP (enhanced green fluorescent protein) [2]. In the present paper we describe this assay and its application to investigating a functional interaction between miR-212 and the 3′UTR of the human inward rectifier K^+ channel $K_{ir}2.1$ [KCNJ2 (potassium inwardly-rectifying channel, subfamily J, member 2)].

It is well known that inwardly-rectifying K^+ channels play an important physiological role in many cell types [3,4]. Down-regulation of these channels contributes significantly to an increased risk of cardiac arrhythmia in the myocardial remodelling process that occurs *en route* to heart failure [5–8]. Chronic alcohol consumption leads to impaired K^+-activated arterial dilation via down-regulation of inward-rectifier K^+ channels, with implications for cerebrovascular disorders [9].

Mechanisms of inward-rectifier K^+ channel down-regulation in myocardial remodelling and alcohol-related arterial dysfunction are not well understood, although some possibilities have been proposed [9–15]. Post-transcriptional regulation of gene expression by miRNAs is a strong possibility that has not been fully investigated.

Inward rectifier K^+ channels are products of the $K_{ir}2$ (*KCNJ*) gene subfamily. $K_{ir}2.1$ (KCNJ2) [16] appears to be the primary component in heart ventricular muscle [17,18] and the sole component in some arterial smooth muscle [19]. Bioinformatics analysis reveals a potential target in the 3′UTR of $K_{ir}2.1$ for miR-212. This miRNA is of particular interest because it is markedly augmented in heart failure [20,21] and in chronic alcoholism [22]. In the present paper we report targeting of $K_{ir}2.1$ and functional down-regulation of inward-rectifier K^+ channels by miR-212.

EXPERIMENTAL

Bioinformatics

The 3′UTRs of $K_{ir}2$ genes were analysed for predicted miRNA target sites by TargetScan [23], MiRanda [24,25] and PicTar [26].

Abbreviations used: CMV, cytomegalovirus; DMEM, Dulbecco's modified Eagle's medium; EGFP, enhanced green fluorescent protein; GAPDH, glyceraldehyde-3-phosphate dehydrogenase; HEK, human embryonic kidney; HPRT1, hypoxanthine–phosphoribosyltransferase 1; $I_{K1,}$ inward-rectifier K^+ current; KCNJ2, potassium inwardly-rectifying channel, subfamily J, member 2; miRNA, microRNA; qRT–PCR, quantitative reverse transcription PCR; RACE, rapid amplification of cDNA ends; siRNA, short interfering RNA; UTR, untranslated region.

[1] These authors contributed equally to this work.

[2] To whom correspondence should be addressed (email anthony.collins@qub.ac.uk).

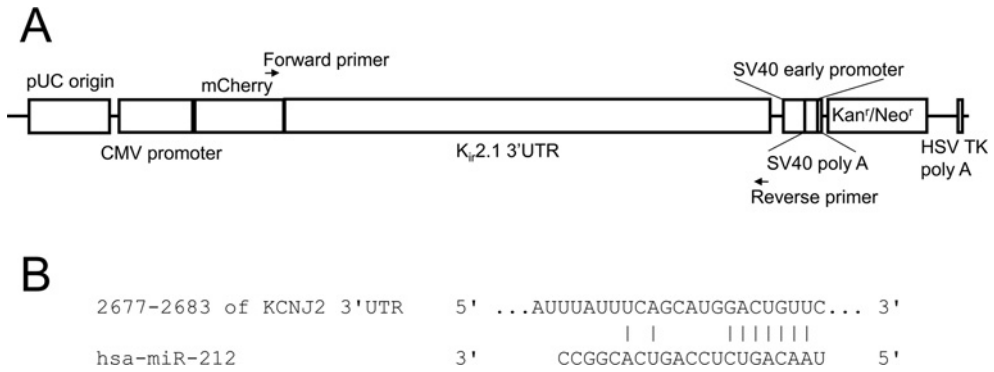

Figure 1 Construct design and predicted target site

(**A**) Structure of pmChKir2.1UTR after linearization with PasI. Location of features: pUC origin of replication, bp 182–825; CMV promoter (human CMV immediate early promoter), bp 908–1486; mCherry (human codon optimized), bp 1510–2229; K_{ir}2.1 3′UTR, bp 2244–6161; SV40 early promoter (and enhancer sequences), bp 6274–6542; SV40 early polyA signals, bp 6441–6576; Kan^r/Neo^r (Kanamycin/neomycin resistance gene), bp 6625–7419; HSV TK polyA (herpes simplex virus thymidine kinase polyadenylation signals), bp 7655–7673; and the primers (5′ ends of complementary), forward bp 2128 and reverse bp 6171. (**B**) Predicted base pairing between miR-212 and the 3′UTR of human K_{ir}2.1 (*KCNJ2*). Upper sequence, bp 2677–2683 of the *KCNJ2* 3′UTR (5′→3′); lower sequence, miR-212 (3′→5′).

Plasmid design and construction

The pmR-mCherry plasmid (Clontech) was modified by removal of 774 bp downstream of the BamHI site in the multiple cloning site following the mCherry stop codon. First, a fragment incorporating bases 2168–2670 of pmR-mCherry was amplified using Phusion® Hot Start II High-Fidelity DNA Polymerase (Fermentas) with the forward primer, 5′-ATATATGGATCCTATGTATCCGCTCATGAGACAATAACCCTG-3′ and the reverse primer, 5′-CCCAAGCGGCCGGAGAAC-3′, and restricted with BamHI and EagI (Fermentas). This was then ligated into the gel-purified 3468 bp fragment generated by restriction of pmR-mCherry with BamHI and EagI. The resulting plasmid was restricted with XhoI (Fermentas) and BamHI and ligated to the 3.9 kb human K_{ir}2.1 3′UTR sequence (GenBank® accession number NM_000891) amplified from human genomic DNA (Bioline) by a two-stage nested PCR using Phusion® Hot Start II High-Fidelity DNA Polymerase and the forward primer (outer), 5′-TGCCCTCACAAGCAAAGAGG-3′; the reverse primer (outer), 5′-CTGCACCTGTCTGTTGAGGC-3′; the forward primer (inner), 5′-AGGTCTCTCGAGCCCTGACATAGACCTTCACAAC-3′; and the reverse primer (inner) 5′-GACAGAGGATCCCATTTCTATGGCTCTATGC-3′, restricted with XhoI and BamHI. The final product (pmChKir2.1UTR) has the CMV (cytomegalovirus) promoter driving transcription of mCherry with the human K_{ir}2.1 3′UTR (Figure 1A). The second stage of the nested PCR was performed with the forward primer, 5′-ATGCCTACTAGTCCCTGACATAGACCTTCACAAC-3′ and the reverse primer, 5′-GACAGAGTCGACCATTTCTATGGCTCTATGC-3′. The product was restricted with SpeI and SalI (Fermentas) and ligated into the NheI (Fermentas) and SalI sites of pmirGLO (Promega), downstream of the firefly luciferase coding sequence, to give pmirGLOKir2.1UTR.

The plasmid pSM30 [2] (encoding EGFP) was used for expression of miRNA and siRNA (short interfering RNA). Complementary pairs of oligonucleotides (25 μM) encoding artificial miRNA and siRNA sequences or a non-targeting negative control sequence (SCR, Invitrogen) [27] were annealed and ligated (T4 DNA ligase, Fermentas) into pSM30 restricted with BsmBI (New England Biolabs). The oligonucleotide sequences used were (mature miRNA/siRNA sequence underlined): hsa-miR-1 (top), 5′-AGCGCTACATACTTCTTTACATTCCATAGTGAAGCCACAGATGTATGGAATGTAAAGAAGTATGTAT-3′; hsa-miR-1 (bottom), 5′-GGCAATACATACTTCTTTACATTCCATACATCTGTGGCTTCACTATGGAATGTAAAGAAGTATGTAG-3′; hsa-miR-212 (top), 5′-AGCGAGCGTGACTGGAGACTGTTATAGTGAAGCCACAGATGTATAACAGTCTCCAGTCACGGCC-3′; hsa-miR-212 (bottom), 5′-GGCAGGCCGTGACTGGAGACTGTTATACATCTGTGGC TTCACTATAACAGTCTCCAGTCACGGCT-3′; SCR (top), 5′-AGCGATCTCCACGCGCAGTACATTTCTAGTGAAGCCA CAGATGTAGAAATGTACTGCGCGTGGAGAC-3′; SCR (bottom), 5′-GGCAGTCTCCACGCGCAGTACATTTCTACATCTGTGGCTTCACTAGAAATGTACTGCGCGTGGAGAT-3′; KCNJ2si (top), 5′-AGCGCAACGAGACTCTTGTCTTCAGTCTAGTGAAGCCACAGATGTAGACTGAAGACAAGAGTCTCGTTT-3′; and KCNJ2si (bottom), 5′-GGCAAAACGAGACTCTTGTCTTCAGTCTACATCTGTGGCTTCACTAGACTGAAGACAAGAGTCTCGTTG-3′.

The KCNJ2si sequence was based on the siRNA reported by Rinne et al. [28]. Following confirmation of inserts by DNA sequencing (Genomics Core, Queen's University Belfast, Belfast, U.K.), plasmids were prepared with a Maxiprep kit (Qiagen) following the manufacturer's instructions. Custom oligonucleotides were purchased from Eurogentech.

Site-directed mutagenesis

An adaptation of the SLIM (site-directed ligase-independent mutagenesis) method [29] was used for mutation of the seed region of the putative miR-212 target site in the human K_{ir}2.1 3′UTR. The pmChKir2.1UTR plasmid (prepared from dam$^+$ *Escherichia coli*) was used as the template in two separate PCRs with Platinum Pfx DNA polymerase (Life Technologies) and 0.5× enhancer buffer. The primers in reaction A were: sense, 5′-GCATGTCAGTGGCATTTGAAACCTTTTTCTAGTTATTAGCGTTT-3′ (mutated bases underlined) and antisense, 5′-TGAAATAAATAACAGAAGAACATAGC-3′. The primers in reaction B were: sense, 5′-AAACCTTTTTCTAGTTATTAGCGTTT-3′ and antisense, 5′-CAAATGCCACTGACATGCTGAAATAAATAACAGAAGAACATAGC-3′ (mutated bases underlined). The methylated template was digested with DpnI (New England Biolabs) to leave the unmethylated mutagenesis product. Reaction products A and B were mixed and re-annealed, then used for transformation of XL-2 Blue

ultracompetent *E. coli* (Agilent). The plasmid preparations (pmChKir2.1UTRm212) were sequenced to confirm the presence of the mutated site (Genomics Core, Queen's University Belfast).

qRT–PCR (quantitative reverse transcription PCR) for miRNA

RNA was extracted using the miRNeasy kit (Qiagen) according to the manufacturers' protocols. RNA (1 μg) was polyadenylated using PAP [poly(A) polymerase; Ambion] at 37 °C for 1 h in a 25 μl reaction mixture. RNA was reverse transcribed with 200 units of SuperScript III reverse transcriptase (Life Technologies) and 0.5 μg of poly(T) adapter (5′-GCGAGCACA-GAATTAATACGACTCACTATAGGTTTTTTTTTTTTVN-3′). The sequence for the miR-212 primer was 5′-ATAACAG-TCTCCAGTCACGGCC-3′. The reverse primer was the 3′ adapter primer: 5′-GCGAGCCACAATTAATACGAC-3′ [3′ RACE (rapid amplification of cDNA ends) outer primer in the FirstChoice RLM-RACE kit, Ambion]. qRT–PCR was performed using Maxima SYBR Green qPCR mastermix (Fermentas) in 10 μl reaction mixtures containing 2 μl of 1:15 cDNA dilution. Reactions were performed on a LightCycler 480 (Roche), with the initial pre-incubation at 50 °C for 2 min and activation at 95 °C for 10 min, followed by 40 cycles at 95 °C for 15 s and 60 °C for 60 s, with fluorescence acquired after 15 s of the 60 °C step. Gene expression data were normalized to 5S RNA. The relative expression was determined as $2^{-\Delta C_t}$, where $\Delta C_t = C_t(\text{miRNA}) - C_t(5S)$.

Production of cell lines stably expressing mCherry–K_{ir}2.1 3′UTR (mChKir2.1UTR cells)

pmChKir2.1UTR was linearized with PasI (Fermentas) (Figure 1) and transfected into HEK (human embryonic kidney)-293 cells using FuGene HD (Roche Diagnostics) in a T25 flask according to the manufacturers' protocol. After 2 days the cells were detached with 0.25 % trypsin/0.9 mM EDTA (Invitrogen), diluted 10-fold into complete medium [DMEM (Dulbecco's modified Eagle's medium), 10 % fetal bovine serum and 1 % Primocin (InvivoGen)] containing 0.3 mg/ml of G418 (Sigma–Aldrich) and re-plated in ten separate aliquots. Red fluorescence was monitored from this time onwards. Cells were maintained for 14 days with replacement of medium every 3–6 days. The G418 concentration was then changed in pairs of cultures to 0.3, 0.4, 0.5, 0.6 and 0.7 mg/ml to determine the optimum selection pressure. At 2–5 days later the cultures were selected for re-plating at single-cell density into 24- or 96-well plates. Wells containing single colonies were selected for propagation after a further 12 days. The mChKir2.1UTR clone used in the present study (clone A4) was selected in 0.7 mg/ml of G418 and subsequently maintained in 0.5 mg/ml of G418.

Genomic incorporation of the intact mCherry-K_{ir}2.1 3′UTR sequence was confirmed by PCR analysis. Genomic DNA was extracted with DirectPCR Lysis reagent (Viagen Biotech) according to the vendor's protocol. The forward primer was in the mCherry coding sequence (5′-ACCTCCCACAACGAGGAC-3′) and the reverse primer was the inner reverse primer used for subcloning as described above (4055 bp product).

Dual fluorescence miRNA targeting assay

HEK-293 cells and mChKir2.1UTR cells were plated on to 8-mm diameter cover slips in a 24-well plate or directly into a 24-well plate. The next day the mChKir2.1UTR cells were transfected with pSM30 containing an insert encoding miR-212, miR-1 or the non-targeting negative control sequence (pSM30-miR-212, pSM30-miR-1 and pSM30-SCR respectively), or MB-IRK3PGEMHE (non-fluorescent negative control plasmid) using JetPEI™ transfection reagent (Polyplus-transfection SA) or FuGene HD transfection reagent (Roche Diagnostics). Cells to be transiently transfected were transfected with either pmChKir2.1UTR or pmChKir2.1UTRm212, in addition to one of pSM30-miR-212, pSM30-miR-1, pSM30-SCR or MB-IRK3PGEMHE using FuGene HD. At 2 days later the coverslips were transferred on to microscope slides for fluorescence microscopy at ×20 magnification using a Nikon Eclipse 80i microscope equipped with G-2A (red) and B-2A (green) filter sets. Cells plated directly into 24-well plates were imaged at ×20 magnification using a Nikon Eclipse TE2000-U microscope equipped with a 488 nm filter (red; mCherry fluorescence) and a 550 nm filter (green; EGFP fluorescence). Red and green images were acquired of multiple fields using NIS Elements software (Nikon). Images in .tif format were analysed by Volocity software (Volocity 5.5.1, PerkinElmer).

We developed a Volocity pipeline for identifying cells in green images and measuring the red and green intensities of each identified cell. The Volocity pipeline identified green cells by intensity. The sum of pixel intensities of each identified cell was then measured. The outlines of the cells were transposed on to the red channel image of the same field and the sum red intensity of each cell was measured. Background fluorescence and cross-channel bleed-through were corrected using images of HEK-293 and mChKir2.1UTR cells transfected with MB-IRK3PGEMHE, HEK-293 cells transfected with pmChKir2.1UTR or pmChKir2.1UTRm212 and MB-IRK3PGEMHE, and non-transfected mChKir2.1UTR cells. Data were exported in Microsoft Excel format for further analysis (Prism 4, GraphPad).

Luciferase assay

HEK-293 cells were seeded in 96-well plates and co-transfected with two plasmids: (i) one of pSM30-SCR or pSM30-miR-212; and (ii) pmirGLOKir2.1UTR, using FuGene HD. At 16–24 h post-transfection, EGFP expression was assessed with a fluorescent light source (Zeiss filter set 09, 450–490 nm excitation, 510 nm beam splitter, 515 nm emission). Dual-Glo® Luciferase assays (Promega) were carried out according to the manufacturer's instructions. Luminescence measurements were made on a plate-reading luminometer (Tristar LB 941, Berthold Technologies).

RT–PCR amplification for HeLa cells

Total mRNA was extracted from HeLa cells grown in a T25 flask (Sigma–Aldrich) with RNeasy Plus Mini kit (Qiagen) and cDNA was generated with random hexamer primers by reverse transcription (Superscript III, Life Technologies) according to the manufacturer's recommendations. The resulting cDNA was subjected to qualitative PCR, which was conducted in a Veriti thermal cycler (Applied Biosystems), and was performed with DreamTaq™ Green DNA Polymerase (Fermentas). Each PCR amplification reaction (50 μl volume) contained 2 μl of HeLa cDNA or 200 ng of human heart genomic DNA (BioChain Institute), 1.25 units of polymerase, 5 μl of dNTP (2 mM each) 5 μl of DreamTaq™ Green buffer and 5 μM of primers. The primer sequences (and predicted fragment sizes) were: K_{ir}2.1 forward, 5′-CGACGTCTATCCTTTCCTGC-3′; K_{ir}2.1 reverse, 5′-TGTGGCATCTTCCCTAAGGT-3′ (278 bp); K_{ir}2.2

forward, 5′-AACCCCTACAGCATCGTGTC-3′; $K_{ir}2.2$ reverse, 5′-GCGATGACCCAGAAGATGAT-3′ (296 bp); 18S (ribosomal RNA) forward, 5′-CCTGCGGCTTAATTTGACTC-3′; and 18S reverse, 5′-ACCAACTAAGAACGGCCATG-3′ (121 bp). The cycling conditions consisted of an initial denaturizing step at 95 °C (60 s) followed by 35 cycles of a thermal step protocol consisting of 95 °C (45 s), 60 °C (20 s) and 72 °C (60 s) and a final step of 72 °C (60 s). A negative control for cDNA was performed without reverse transcription (− RT control). An aliquot (10 μl) of the RT–PCRs were analysed by electrophoresis on a 1.5 % agarose and 0.3 μg/ml ethidium bromide gel in TBE (Tris/borate/EDTA).

Quantitative PCR was carried out using TaqMan® Gene Expression assays (Life Technologies): Hs01003267_m1 [HPRT1 (hypoxanthine–phosphoribosyltransferase 1); Hs99999905_m1 [GAPDH (glyceraldehyde-3-phosphate dehydrogenase)]; and Hs00265315_m1 (KCNJ2), following reverse transcription with a high-capacity kit (catalogue number 4374966, Life Technologies).

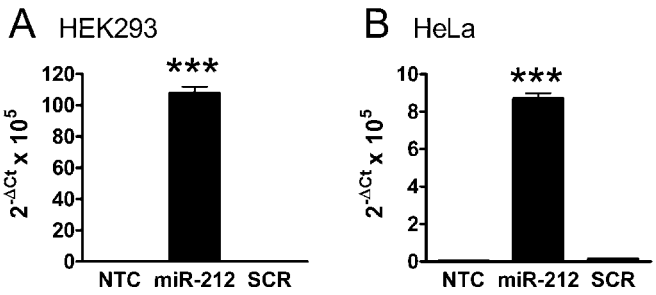

Figure 2 Expression of mature miR-212 in pSM30-miR-212-transfected cells

HEK-293 (**A**) and HeLa (**B**) cells were transfected with pSM30-miR-212 (miR-212) or pSM30-SCR (SCR). High-efficiency transfection was confirmed by monitoring green fluorescence. RNA was extracted and qRT–PCR was performed with a miR-212-specific primer as described in Experimental section. A negative control (NTC) was performed without template. The fold difference relative to 5S RNA is expressed as $2^{-\Delta C_t}$ (means ± S.E.M.). ***$P < .001$ for miR-212 compared with SCR and NTC as determined by one-way ANOVA on the ΔC_t values; $n = 3$.

Immunoblotting of HeLa cell extracts

Following transfection, the plasma membrane was isolated from HeLa cells for Western blotting. Cells were scraped in PBS and pelleted at 1000 ***g*** for 5 min at 4 °C. The cell pellet was resuspended in 20 mM Mops, 250 mM sucrose, 1 mM PMSF, 0.1 mM EDTA, 50 mM sodium fluoride and 2 mM sodium vanadate and snap frozen with liquid nitrogen to break the cell membranes. The samples were then homogenized with a Biospec Tissue Tearor for 2×20 s then sonicated for 2×15 s. Samples were centrifuged at 200 ***g*** for 5 min at 4 °C to pellet unbroken cells and nuclei, and the supernatant was ultracentrifuged at 40000 rev./min for 1 h at 4 °C in a Beckman TL 100 rotor to pellet the membrane fraction. The membrane pellet was then resuspended in NuPAGE LDS buffer (Invitrogen), sonicated for 30 s and boiled for 5 min. Membrane samples were resolved by SDS/PAGE (12 % gel) and transferred by electrophoresis on to PVDF membranes. The membrane-bound protein was probed with anti-$K_{ir}2.1$ antibody (1:500 dilution; Abcam) followed by anti-(mouse horseradish peroxidase-conjugated) secondary antibody (1:1000 dilution; Santa Cruz Biotechnology). Equivalent loading of protein was checked by probing with an antibody against Na/K-ATPase α1 (1:500 dilution; Santa Cruz Biotechnology). Blots were imaged on a UVP Autochemi system.

Electrophysiology

Inward-rectifier K^+ current was measured by patch-clamp recording. HeLa cells were seeded on to coverslips 24 h after transfection with pSM30-miR-212, pSM30-SCR or the pSM30-based siRNA plasmid (pSM30-KCNJ2si) and allowed to grow in complete DMEM for a further 18–24 h. Coverslips were then transferred to a 2 ml recording chamber mounted on the stage of an inverted microscope (Axiovert 100, Zeiss) equipped with a fluorescent light source. Cells were superfused with normal Tyrode solution (in mM: 140 NaCl, 4 KCl, 2.5 $CaCl_2$, 1 $MgCl_2$, 10 glucose and 10 Hepes, pH 7.4 with NaOH) at 22 °C. Whole-cell currents were recorded from fluorescent cells in voltage-clamp mode using an Axopatch 200B amplifier (Molecular Devices) grounded to the recording chamber via a 3 M KCl agar bridge. Electrodes (1–4 MΩ) were pulled from filamented borosilicate glass capillaries (1.5 mm outside diameter and 1.12 mm inside diameter; World Precision Instruments). The internal pipette solution was K^+-based [in mM: 65 KCl, 40 KF, 5 EGTA, 10 glucose, 0.24 $NaVO_3$, 10 Hepes, 5 tetrasodium pyrophosphate and 15 KOH (pH 7.4)]. Reversal potentials and normalized current densities were corrected for the pipette junction potential (7.8 mV) offline. Access resistance was typically 2–8 MΩ and cell capacitances were 39 ± 4 pF as assessed by the membrane-test facility of Clampex 10.2 (Molecular Devices). Both access resistance and cell capacitance were compensated using the amplifier (∼80 %); currents were filtered at 10 KHz and normalized to capacitance for comparison of the current density.

Prior to recording membrane current using an ascending voltage ramp protocol (− 100 to + 50 mV, 60 mV/s; applied every 5 s after an initial 200 ms step to − 100 mV to allow for inactivation of any hyperpolarization-activated or uncompensated capacitative current) the external solution was switched via a rapid-solution device positioned adjacent to the cell (ALA Scientific Instruments) to one containing 120 mM K^+ [in mM: 115 KCl, 20 NaCl, 2.5 $CaCl_2$, 1 $MgCl_2$, 10 glucose, 10 Hepes and 5 KOH (pH 7.4)] resulting in a predicted E_K of − 3.9 mV. I_{K1} (inward-rectifier K^+ current) was isolated as the current sensitive to application of 100 μM Ba^{2+} in the external solution.

Statistical methods

Statistical analysis was performed with Prism 4.0 software (GraphPad). Student's *t* test was used for comparing two groups. ANOVA was used for comparing more than two groups.

RESULTS

Bioinformatics analysis

MiR-212 was predicted to target the 3′UTR of human $K_{ir}2.1$ by TargetScan [23] and MiRanda [24]. Predicted base-pairing between miR-212 and the target sequence is shown in Figure 1(B).

Expression of exogenous miRNA in HEK-293 and HeLa cells

The ability of the pSM30 system to direct expression of a mature miRNA was confirmed by qRT–PCR as shown in Figure 2. Transfection with pmiR-212 increased expression of mature miR-212 in HEK-293 (Figure 2A) and in HeLa (Figure 2B) cells.

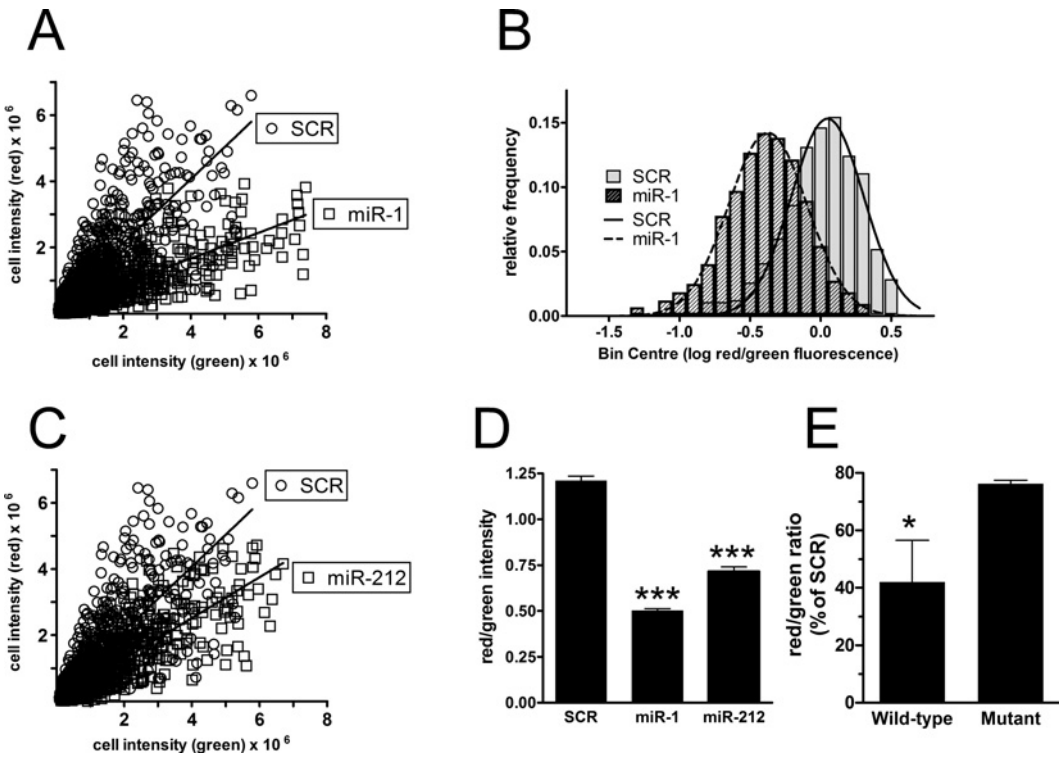

Figure 3 Results of image analysis two days after co-transfection of HEK-293 cells

Down-regulation of mCherry-K_{ir}2.1 3′UTR by pSM30-miR-1 and pSM30-miR-212, and attenuation of the miR-212 effect by mutation of the putative seed region. (**A**) Green compared with red integrated fluorescence intensity of cells transfected with pSM30-SCR (○) and pSM30-miR-1 (□). Lines are linear regressions. (**B**) Relative frequency histograms of log red/green intensity ratios derived from the data in (**A**). Lines are fits of Gaussian distributions. (**C**) Green compared with red integrated fluorescence intensity of cells transfected with pSM30-SCR (○) and pSM30-miR-212 (□). Results are from the same experiment as (**A**) and are presented in a separate panel for ease of viewing; pSM30-SCR data are the same in (**A**) and (**C**). Lines are linear regressions. (**D**) Red/green intensity ratios (means ± S.E.M.) for pSM30-SCR-, pSM30-miR-1- and pSM30-miR-212-transfected cells. Log-transformed data were compared by one-way ANOVA; $***P < 0.001$ for miR-1 compared with SCR and miR-212 compared with SCR; $n = 731$ (SCR), 776 (miR-1) and 550 (miR-212). (**E**) Red/green ratio in pSM30-miR-212-transfected cells as a percentage of red/green ratio in pSM30-SCR-transfected cells (means ± S.E.M.). Co-transfections were with pmChKir2.1UTR (Wild-type) or pmChKir2.1UTRm212 (Mutant). $*P < .05$ as determined by Student's t test on the log-transformed percentage decrease for 3 independent experiments.

Dual-fluorescence assay

If a microRNA co-expressed with EGFP targets the 3′UTR cloned downstream of the red fluorescent protein coding sequence (mCherry) we would expect to observe a decrease in red fluorescence and a concomitant reduction in the ratio of red/green fluorescence. HEK-293 cells were therefore co-transfected with pmChKir2.1UTR and a pSM30-based plasmid expressing either miR-1 or a non-targeting miRNA control (SCR). The total green and red intensities of multiple cells were measured using fluorescent microscopy and the values for each cell plotted against each other (Figure 3A). Comparison of the lines of best fit clearly illustrates the expected reduction in red fluorescence in those cells overexpressing miR-1 compared with the non-targeting miRNA. Similarly, the relative frequency histograms of log red/green fluorescence ratios for cells transfected with pmChKir2.1UTR/pSM30-miR-1 are shifted to the left-hand side relative to those for cells transfected with pmChKir2.1UTR/pSM30-SCR (Figure 3B). A plot of red compared with green intensity for cells transfected with pmChKir2.1UTR/pSM30-miR-212 and pmChKir2.1UTR/pSM30-SCR is shown in Figure 3(C). Red/green fluorescence was significantly lower for pmChKir2.1UTR/pSM30-miR-1-transfected and pmChKir2.1UTR/pSM30-miR-212-transfected compared with the pmChKir2.1UTR/pSM30-SCR-transfected cells (Figure 3D).

Mutation analysis of the putative miR-212 target site

To confirm that the reduction in red fluorescence observed following overexpression of miR-212 is mediated through the predicted target site, we tested whether this effect could be prevented by mutating the sequence of the site to disrupt binding to the miR-212 seed region. The percentage of red/green fluorescence ratio in pSM30-miR-212- compared with pSM30-SCR-transfected cells was significantly lower in cells carrying the wild-type (pmChKir2.1UTR) compared with the mutated (pmChKir2.1UTRm212) construct (Figure 3E), demonstrating that the mutation attenuated the sensitivity to miR-212.

Dual-fluorescence assay in stably transfected mChKir2.1UTR cells

The use of a reporter plasmid in addition to the miRNA expression vector has some potential drawbacks. For example variations in transfection efficiency may introduce noise that multiplies with the number of co-transfected constructs. A strategy that employs single transfections may abrogate this problem. We therefore generated a cell line stably transfected with the mCherry reporter linked with the K_{ir}2.1 3′UTR (mChKir2.1UTR cells). This was confirmed by PCR analysis of genomic DNA. Figure 4(A) shows an agarose ethidium bromide electrophoresis gel of PCR products from mChKir2.1UTR genomic DNA (lane 2), untransfected

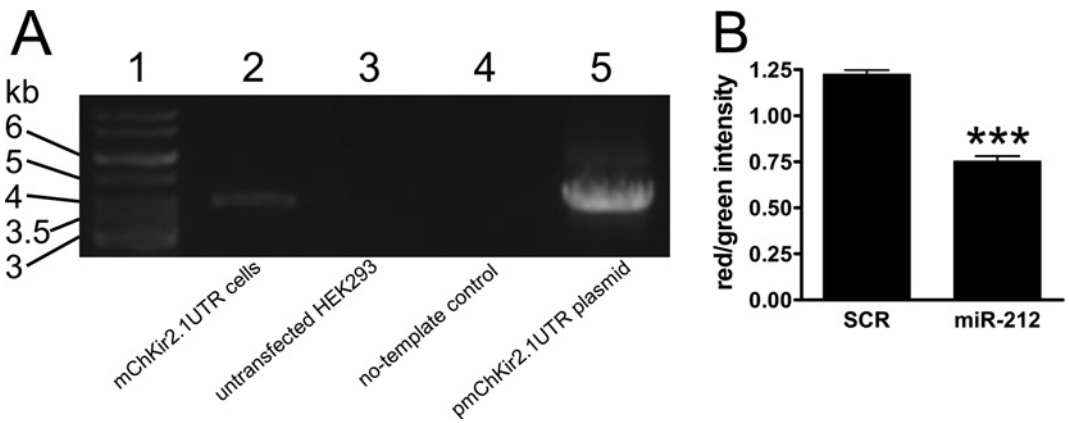

Figure 4 Characterization of stably transfected mChKir2.1UTR cells and down-regulation of mCherry-K_{ir}2.1 3′UTR expression by miR-212

(**A**) Confirmation of integration of the mCherry-Kir2.1 3′UTR construct in the genome of mChKir2.1UTR cells. Agarose ethidium bromide electrophoresis of PCRs using primers described in the Experimental section and templates as follows: lane 2: mChKir2.1UTR genomic DNA; lane 3: HEK293 genomic DNA; lane 4: no-template control; lane 5: pmChKir2.1UTR plasmid. (**B**) Down-regulation of mCherry expression in mChKir2.1UTR cells by miR-212. Red/green intensity ratios (means ± S.E.M.) for pSM30-SCR-transfected (SCR) and pSM30-miR-212-transfected (miR-212) cells. Log-transformed data were compared by Student's *t* test; $***P < 0.001$; $n = 801$ (SCR) and 478 (miR-212).

HEK-293 genomic DNA (lane 3), no-template control (lane 4) and pmChKir2.1UTR plasmid (lane 5). The forward primer site is in the mCherry coding sequence and the reverse primer site is at the end of the K_{ir}2.1 3′UTR sequence (Figure 1A). The bands in lanes 2 and 5 are consistent with the predicted product size of 4055 bp. These data confirm the presence of the K_{ir}2.1 3′UTR downstream of the mCherry coding sequence in the genomic DNA of mChKir2.1UTR cells.

Down-regulation of mCherry expression by miR-212 in mChKir2.1UTR cells is shown in Figure 4(B). Dual-fluorescence analysis was performed as described above. Red/green fluorescence was significantly lower for pSM30-miR-212-transfected compared with the pSM30-SCR-transfected cells. These data again indicate targeting of the K_{ir}2.1 3′UTR by miR-212.

Luciferase assay

The novel miR-212 result from the dual-fluorescence assay suggested that a similar result may be obtained with a more traditional luciferase-based assay. The effect of miR-212 on the expression of firefly luciferase with the K_{ir}2.1 3′UTR is shown in Figure 5. Firefly luciferase activity (normalized to *Renilla* luciferase) was less for pSM30-miR-212- than pSM30-SCR-transfected cells.

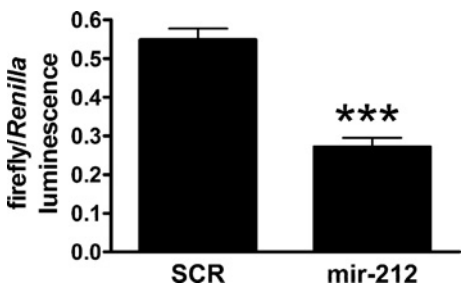

Figure 5 Assessment of miR-212 targeting by luciferase assay

HEK-293 cells were transfected with pmirGLOKir2.1UTR and pSM30-SCR or pSM30-miR-212. Firefly and *Renilla* luciferase activities were determined using the Dual-Glo® Luciferase assay. Data are expressed as firefly luciferase activity normalized to *Renilla* luciferase activity (means ± S.E.M.). $***P < .001$ as determined by Student's *t* test on log-transformed data; $n = 6$.

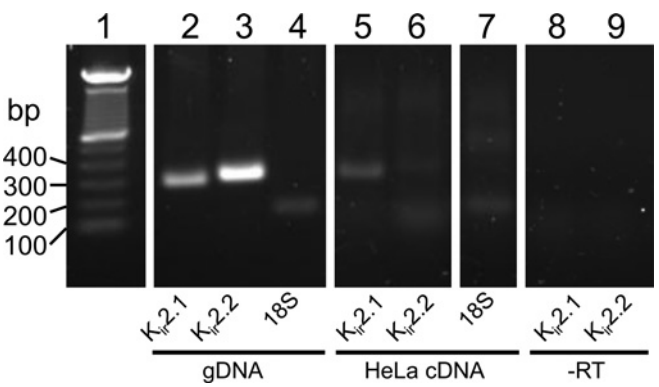

Figure 6 Endogenous expression of K_{ir}2.1 in HeLa cells

RT–PCR was performed on RNA extracted from HeLa cells (lanes 5–7). Negative controls were performed without reverse transcription (lanes 8 and 9; − RT). PCR was performed on human genomic DNA (lanes 2–4; gDNA). Primers were specific for human K_{ir}2.1 (lanes 2, 5 and 8), human K_{ir}2.2 (lanes 3, 6 and 9) and 18S ribosomal RNA (lanes 4 and 7). Reaction products were analysed by agarose ethidium bromide gel electrophoresis.

Down-regulation of endogenous K_{ir}2.1 protein by miR-212

The results of the dual-fluorescence assay predicted that miR-212 would suppress the expression of endogenous K_{ir}2.1. We first confirmed the expression of K_{ir}2.1 mRNA in HeLa cells, as shown by the results of RT–PCR experiments shown in Figure 6. Primers were designed to amplify K_{ir}2.1, K_{ir}2.2 and 18S ribosomal RNA. Human genomic DNA was used as a positive control for these primers (lanes 2–4). PCR products from HeLa cDNA are shown in lanes 5–7. There was clearly a product for K_{ir}2.1 (lane 5) and a very faint product for K_{ir}2.2 (lane 6) despite a strong signal with the K_{ir}2.2 primers from the genomic DNA template (lane 3).

MicroRNAs have been reported to promote degradation of the target mRNA in some cases. We performed qPCR to determine whether miR-212 caused a reduction of K_{ir}2.1 mRNA in HeLa cells. As shown in Figure 7, miR-212 expression did not significantly change K_{ir}2.1 mRNA content relative to two different

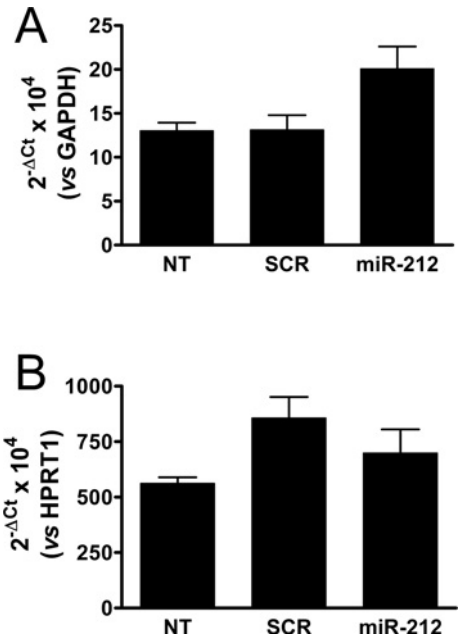

Figure 7 No effect of miR-212 on $K_{ir}2.1$ mRNA in HeLa cells

RNA extraction, reverse transcription and quantitative PCR (TaqMan®) were carried out on non-transfected HeLa cells (NT) and HeLa cells transfected with pSM30-SCR (SCR) or pSM30-miR-212 (miR-212). Data are expressed as $2^{-\Delta C_t}$ where $\Delta C_t = C_t(KCNJ2) - C_t$(control gene). The control genes were GAPDH (**A**) and HPRT1 (**B**). $P > 0.05$ by ANOVA.

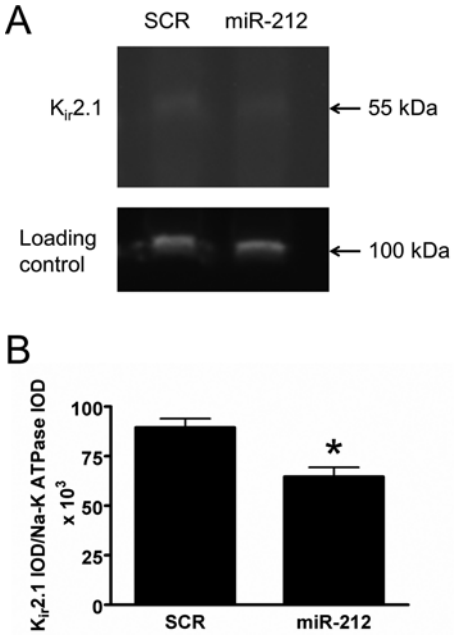

Figure 8 Down-regulation of $K_{ir}2.1$ protein expression by miR-212

HeLa cells were transfected with pSM30-SCR (SCR) or pSM30-miR-212 (miR-212) before extraction of membrane proteins and analysis by SDS/PAGE and immunoblotting. (**A**) Immunoblot probed with anti-$K_{ir}2.1$ and anti-(Na^+/K^+-ATPase $\alpha 1$) (loading control) antibodies. (**B**) Intensity of $K_{ir}2.1$ relative to Na^+/K^+-ATPase $\alpha 1$ (*$P < 0.05$ for three independent experiments).

endogenous control genes, *GAPDH* (Figure 7A) and *HPRT1* (Figure 7B). Despite the lack of effect at the mRNA level, miR-212 did down-regulate endogenous $K_{ir}2.1$ protein in HeLa cells. Figure 8(A) shows an example of a Western blot of membrane extracts from HeLa cells transfected with pSM30-miR-212 or pSM30-SCR, probed with antibodies against $K_{ir}2.1$ and Na^+/K^+-ATPase $\alpha 1$ subunit (loading control). Figure 8(B) summarizes the data from three such experiments and shows that miR-212 reduced $K_{ir}2.1$ protein.

Down-regulation of I_{K1} by miR-212

We sought further evidence for targeting of $K_{ir}2.1$ by miR-212 by investigating the effect on inward-rectifier K^+ channel activity itself in HeLa cells. Green fluorescent HeLa cells were selected 48 h post-transfection with pSM30-miR-212 or pSM30-SCR for measurement of inwardly-rectifying K^+ current using the patch-clamp technique. Voltage ramps (-100 mV to $+50$ mV at 60 mV/s; Figure 9A) applied from a holding potential of -40 mV resulted in a current which was inward at negative voltages and reversed close to 0 mV (see Figure 9Bi; ctrl). Application of 100 μM Ba^{2+} (a relatively selective inhibitor of inward rectifier K^+ channels [30–33]) inhibited portions of both the inward and outward whole-cell current with preferential inhibition of the inward portion (Figure 9Bi; Ba^{2+}). On average the current at -108 mV (corrected for pipette junction potential) recorded in pSM30-SCR transfected cells was reduced from -219.02 ± 47.61 pA/pF to -178.71 ± 47.79 pA/pF by the application of 100 μM Ba^{2+} (Figure 9Ci; $n = 8$; $P < 0.01$ determined by paired Student's t test). As plotted in Figure 9(D) the Ba^{2+}-sensitive current exhibited strong inward rectification and reversed at -3.55 ± 2.61 mV. In cells transfected with pSM30-miR-212 the whole-cell inward current was smaller in amplitude to that in cells transfected with pSM30-SCR (Figure 9Bii). On average the current at -108 mV (corrected for pipette junction potential) recorded in pSM30-miR-212-transfected cells was reduced from -104.98 ± 41.07 pA/pF to -100.91 ± 41.10 pA/pF by the application of 100 μM Ba^{2+} (Figure 9Cii; $n = 13$; $P < 0.01$ determined by paired Student's t test). The Ba^{2+}-sensitive current in cells transfected with pSM30-miR-212 was significantly smaller than the equivalent current in pSM30-SCR-transfected cells (Figure 9D; $P < 0.01$ determined by ANOVA for the entire IV relationship). Transfection with pSM30-KCNJ2si also reduced the Ba^{2+}-sensitive current [Figure 9E; $P < 0.01$ determined by ANOVA for the entire IV (current–voltage) relationship].

DISCUSSION

We present a novel dual-fluorescence assay for identifying miRNA–target interactions. We also provide the first evidence that miR-212 can down-regulate $K_{ir}2.1$ expression and significantly alter I_{K1} density.

Advantages of the dual-fluorescence system

Luciferase-based assays have been widely used for investigating miRNA–target interactions. In our hands, and anecdotally in the hands of others, they tend to be highly variable, necessitating time-consuming optimization of conditions. They also require cell lysis, leading to loss of information. Large sample sizes are impractical because each transfected well yields only one data point and the required reagents tend to be quite expensive. The dual-fluorescence assay yields a data point for each cell, of which there are typically several hundred in an experiment. A large sample size enables the detection of subtle effects of the miRNA of interest and comparisons of the relative efficacy of different

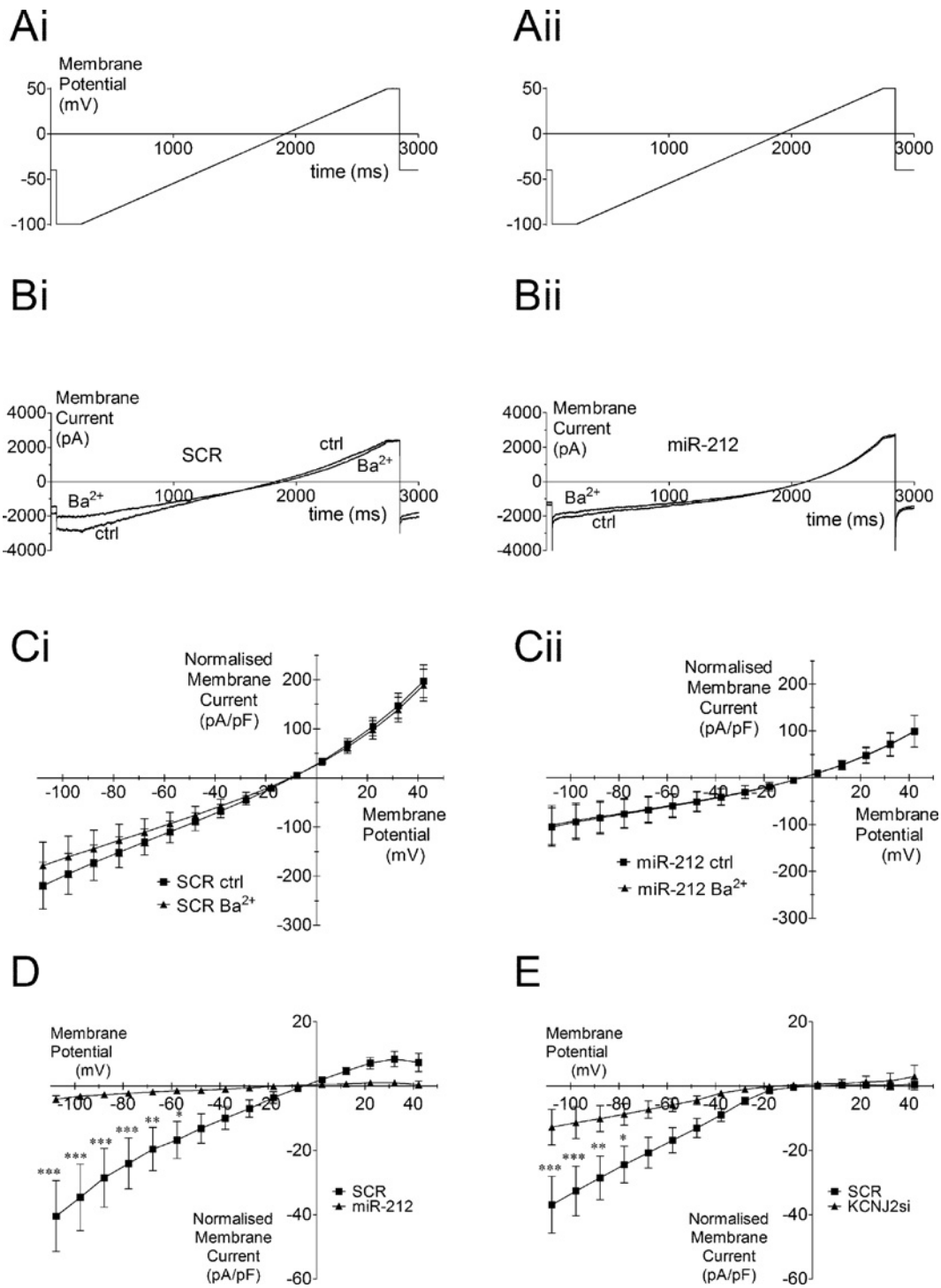

Figure 9 Inward-rectifier K^+ currents in HeLa cells transfected with pSM30-miR-212, pSM30-KCNJ2si or pSM30-SCR

(**A**) The voltage protocol used to elicit currents. (**B**) Whole-cell currents elicited in the absence (ctrl) and presence of 100 μM Ba^{2+} (Ba^{2+}) in cells 48 h after transfection with pSM30-SCR (i) and pSM30-miR-212 (ii). (**C**) Mean $\pm$ S.E.M. whole-cell current-densities (normalized to cell capacitance and corrected for junction potential) recorded in 8 cells transfected with pSM30-SCR (i) and 13 cells transfected with pSM30-miR-212(ii). (**D**) Mean $\pm$ S.E.M. Ba^{2+}-sensitive current densities for pSM30-SCR- and pSM30-miR-212-transfected cells. (**E**) Mean $\pm$ S.E.M. Ba^{2+}-sensitive current densities for pSM30-SCR- ($n = 11$) and pSM30-KCNJ2si-transfected ($n = 10$) cells.*$P < 0.05$, **$P < 0.01$ and ***$P < 0.001$ as determined by ANOVA with a Bonferroni-corrected ad hoc test.

miRNAs. It also reduces the reliance on assumptions when testing for statistical significance. Luciferase data are typically expressed as the ratio reporter/normalizer (e.g. luciferase/β-galactosidase or firefly/*Renilla*) and tested for significance using a parametric test such as Student's t test. Such tests rely on the assumption of a Gaussian distribution. The larger sample sizes achievable with our dual-fluorescence assay enable the construction of a frequency histogram (Figure 3B), allowing the direct assessment of the degree of approximation to a Gaussian distribution. Results of parametric tests can then be viewed with greater confidence.

Measurement of fluorescence is minimally invasive for the cell so the dual-fluorescence assay could be readily adapted for time-course studies. We anticipate that it could also be scaled up and adapted for flow cytometry, which would give a higher sensitivity associated with larger sample sizes. Further modifications such as more efficient methods for producing stably transfected cell lines [e.g. ViraPower™, Flp-In™ (Life Technologies)] and robotic sample handling may make the assay suitable for high-throughput screening of miRNA–target interactions.

The method described in the present paper requires an investment of time and effort in the construction of the miRNA expression plasmid, but once cloned the construct can be used indefinitely in future for assays against any sequences of interest. Part of our planned future work is to develop a catalogue of miRNA expression plasmids for this purpose. In its present form the method also involves an investment of labour in the acquisition of images. Throughput could be increased by the use of a high-content analysis system. The available software is able to analyse multiple images automatically so the image analysis is not onerous. The results of the present study were analysed with Volocity software. The method also works well with CellProfiler software [34], which is available via free download.

We used the luciferase-based Dual-Glo® assay to validate the miR-212 result (Figure 5). We also used the Dual-Light® system (Applied Biosystems) with similar results (results not shown). These data were obtained with considerable time and resources expended on optimizing the conditions, which was in part the motivation for investigating an alternative assay. We anticipated that the variability of luciferase-based assays may be due to the requirement for transfection with multiple constructs simultaneously. However, we found the pmChKir2.1UTR/pSM30 transient co-transfection version of the dual-fluorescence assay to be surprisingly reliable. Nevertheless we developed the mChK_{ir}2.1UTR stably transfected cell line with a view to reducing any inter-experimental variability associated with double transfections. We again found down-regulation of mCherry-K_{ir}2.1 3′UTR by miR-212 using this single transfection approach (Figure 4B).

miRNA target sites in the Kir2.1 3′ UTR

In this study we used the dual-fluorescence assay to confirm the known miR-1 target in the K_{ir}2.1 3′ UTR [35] (Figures 3A, 3B and 3D) and to identify a novel target of miR-212 (Figures 3C and 3D). The inhibitory effect of miR-212 on mCherry-K_{ir}2.1 3′ UTR expression was significantly attenuated by mutation of the seed region of the predicted miR-212 target site (Figure 3E), supporting the notion that this is indeed a functional site.

Validation of pSM30 as a miRNA expression reporter vector

pSM30 is a miRNA expression plasmid designed by Dr G. Du (University of Texas Health Science Center at Houston, Houston, TX, U.S.A.; [2]) into which an artificial miRNA sequence of choice can be inserted within an artificial intron of the *EGFP* gene. The advantages of this method are that miRNAs are efficiently transcribed and processed by the cell's own machinery, and expression can be monitored by the simultaneous expression of EGFP which (unlike conventional expression reporter vectors) is expressed only if the miRNA insert is correctly spliced. We have confirmed expression of the mature miRNA in pSM30-miR-212-transfected cells by quantitative PCR (Figure 2). The dual-fluorescence method takes advantage of the co-expression of EGFP and mature miRNA in transfected cells.

Down-regulation of endogenous K_{ir}2.1 by miR-212

Having demonstrated an inhibitory effect of miR-212 on the K_{ir}2.1 3′UTR in reporter systems (Figures 3–5), we investigated the effect of miR-212 on the expression of endogenous K_{ir}2.1. The results of quantitative PCR experiments (Figure 7) indicated that miR-212 did not suppress K_{ir}2.1 mRNA, although a decrease in K_{ir}2.1 protein was seen (Figure 8). The effect of miR-212 on K_{ir}2.1 expression therefore appears to be mediated through inhibition of protein translation rather than mRNA degradation.

Functional down-regulation of I_{K1} by miR-212

We have also shown that miR-212 expression inhibited inward-rectifier K^+ channel function. Inward-rectifier K^+ channels were previously identified in HeLa cells [36] and later characterized as K_{ir}2.1 [37]. We confirmed the presence of K_{ir}2.1 mRNA in HeLa cells by PCR (Figure 6). This stable endogenous expression in an easily transfected cell line made HeLa cells ideal candidates for investigation of the functional regulation of K_{ir}2.1 by miR-212. Transfection of HeLa cells with pSM30-miR-212 did indeed reduce I_{K1} density, as demonstrated by whole-cell recording (Figure 9). This was most likely to be due to reduced expression of K_{ir}2.1 (Figure 8), although we cannot rule out a minor contribution from K_{ir}2.2 which was detected faintly by PCR of HeLa cDNA (Figure 6) and is predicted to be targeted by miR-212 (by TargetScan, MiRanda and PicTar). This would also be consistent with the apparently smaller effect of KCNJ2si on HeLa I_{K1} density compared with miR-212 (Figures 9D and 9E). The possibility of miR-212 regulating both K_{ir}2.1 and K_{ir}2.2 is an important subject for future study because there is evidence that K_{ir}2.2 contributes significantly to the cardiac I_{K1} [17,38–40].

The effect of miR-212 on I_{K1} density was greater than the effect of miR-212 on red/green fluorescence (Figures 3 and 4) and endogenous K_{ir}2.1 protein (Figure 8). This may be due to the selection of highly expressing cells for patch-clamp, the over-expression of target protein in the dual-fluorescence assay and the background level of K_{ir}2.1 protein from untransfected cells. The difference in rectification of the control Ba^{2+}-sensitive current shown in Figures 9(D) and 9(E) is probably due to a subtle difference in recording conditions. In Figure 9(D) Ba^{2+} was applied after run-up of outward current which was probably a result of washout of intracellular polyamines [41–43]. In Figure 9(E), in the interests of time, Ba^{2+} was applied earlier in the recording.

miR-212 and K_{ir}2.1 in health and disease

MiR-212 is one of the most up-regulated miRNAs (8.1-fold) in human heart failure [21]. Its targeting of K_{ir}2.1 is of interest because K_{ir}2.1 is considered to be the major component of cardiac I_{K1} [17,18]. Down-regulation of I_{K1} contributes to the risk of cardiac arrhythmia during the process of myocardial remodelling en route to heart failure [5–7,44]. MiR-1 has been identified as important in down-regulating I_{K1} in acute myocardial infarction [35], but miR-1 is not consistently up-regulated in chronic human cardiomyopathy, being found to be actually decreased in four [45–48] and unchanged in one out of seven studies [49].

Inward-rectifier K^+ channels have an important role in regulating vascular tone in small cerebral arteries such as the basilar artery [19,50]. Chronic alcohol consumption is associated with dysfunction of the cerebral vasculature [51–53], which may contribute to cerebrovascular disorders seen in alcoholism [54]. K_{ir}2.1 may be involved, as inward-rectifier K^+ channel activity and K_{ir}2.1 protein were reduced in basal arteries of alcohol-fed

rats [9]. Interestingly, miR-212 was up-regulated 20-fold in colon biopsy samples from alcoholics [22]. The effect of alcohol on miR-212 expression in basilar artery is unknown, but it would be intriguing to investigate the possible link between miR-212 and $K_{ir}2.1$ in alcohol-induced basilar artery dysfunction.

The miR-212 target site in the $K_{ir}2.1$ 3′UTR was predicted by TargetScan and MiRanda, but not by PicTar. The different prediction algorithms do not agree with each other in many instances, illustrating the need for an efficient functional assay for identifying miRNA target sites unequivocally. The miR-212 site is classified as poorly conserved by TargetScan, although it is conserved across sixteen of the listed mammalian species. We decided to focus on miR-212 over other miRNAs because of its dramatic up-regulation in conditions that are characterized by a decrease in inward-rectifier K^+ channel function, as discussed above. Thus we approached the issue from a physiological perspective and used bioinformatics as a tool, rather than using the bioinformatics analysis as a starting point.

miRNA-based therapy

The results of the present study identify miR-212 as a candidate regulator of $K_{ir}2.1$ expression. Future studies may show a functional link between miR-212 and $K_{ir}2.1$ in diseases such as heart failure and the cerebrovascular complications of alcoholism. MiR-212 would then become a potential therapeutic target. Until very recently the use of miRNA-based therapy seemed a distant prospect; however, Montgomery et al. [55] have used an 'antagomir' to improve cardiac function and survival in Dahl hypertensive rats. Others have employed a viral vector (AAV9)-dependent approach to successfully and relatively selectively target short hairpin RNA molecules to the heart in rodents [56]. In terms of therapeutic value for humans the first human clinical trials of miRNA inhibition are underway (Santaris Pharma; www.clinicaltrials.gov).

Summary

We have presented a novel assay for identifying functional interactions between miRNAs and a 3′UTR. Further refinements could make the assay suitable for high-throughput screening. We have shown that a strategy that combines analysis of genes likely to be responsible for a pathogenic phenotype with those miRNAs altered in the same disease is an effective way to identify functional interactions. Specifically, the down-regulation of $K_{ir}2.1$ in heart failure and alcoholic cerebrovascular dysfunction may be functionally linked to the up-regulation of miR-212.

AUTHOR CONTRIBUTION

Dana Goldoni performed plasmid design and construction, the luciferase assays, RT–PCRs and electrophysiology experiments; Janet Yarham performed the dual fluorescence miRNA targeting assay; Mary McGahon performed electrophysiology experiments; Anna O'Connor performed plasmid design and construction; Jasenka Guduric-Fuchs performed RT–PCRs; Kevin Edgar and Denise McDonald performed immunoblotting. David Simpson performed plasmid design and RT–PCRs. Anthony Collins performed the bioinformatics analysis, plasmid design and construction, site-directed mutagenesis, production of the cell lines, luciferase assays and electrophysiology experiments. All authors contributed to the experimental conception and design and helped critique the output for important intellectual content.

ACKNOWLEDGEMENTS

We thank Dr G. Du for kindly providing pSM30; Ms L. Colhoun for assistance with fluorescence microscopy and Mr A. Devine for assistance with the Volocity software.

FUNDING

This work was supported by The British Heart Foundation [grant number PG110/039/28365 (to A.C. and D.A.S.)] and the BBSRC (Biotechnology and Biological Sciences Research Council) [grant number BB/H005498/1 (to D.A.S.)].

REFERENCES

1 Shah, A. A., Meese, E. and Blin, N. (2010) Profiling of regulatory microRNA transcriptomes in various biological processes: a review. J. Appl. Genet. **51**, 501–507
2 Du, G., Yonekubo, J., Zeng, Y., Osisami, M. and Frohman, M. A. (2006) Design of expression vectors for RNA interference based on miRNAs and RNA splicing. FEBS J. **273**, 5421–5427
3 de Boer, T. P., Houtman, M. J., Compier, M. and van der Heyden, M. A. (2010) The mammalian $K_{IR}2.x$ inward rectifier ion channel family: expression pattern and pathophysiology. Acta Physiol. **199**, 243–256
4 Hibino, H., Inanobe, A., Furutani, K., Murakami, S., Findlay, I. and Kurachi, Y. (2010) Inwardly rectifying potassium channels: their structure, function, and physiological roles. Physiol. Rev. **90**, 291–366
5 Beuckelmann, D. J., Nabauer, M. and Erdmann, E. (1993) Alterations of K^+ currents in isolated human ventricular myocytes from patients with terminal heart failure. Circ. Res. **73**, 379–385
6 Li, G. R., Lau, C. P., Leung, T. K. and Nattel, S. (2004) Ionic current abnormalities associated with prolonged action potentials in cardiomyocytes from diseased human right ventricles. Heart Rhythm **1**, 460–468
7 Pogwizd, S. M., Schlotthauer, K., Li, L., Yuan, W. and Bers, D. M. (2001) Arrhythmogenesis and contractile dysfunction in heart failure: roles of sodium-calcium exchange, inward rectifier potassium current, and residual β-adrenergic responsiveness. Circ. Res. **88**, 1159–1167
8 Rose, J., Armoundas, A. A., Tian, Y., DiSilvestre, D., Burysek, M., Halperin, V., O'Rourke, B., Kass, D. A., Marban, E. and Tomaselli, G. F. (2005) Molecular correlates of altered expression of potassium currents in failing rabbit myocardium. Am. J. Physiol. Heart Circ. Physiol. **288**, H2077–H2087
9 Sun, H., Fang, Q. and Mayhan, W. G. (2004) Inward rectifier potassium channels in the basilar artery during chronic alcohol consumption. Alcohol Clin. Exp. Res. **28**, 1557–1561
10 Fauconnier, J., Lacampagne, A., Rauzier, J. M., Vassort, G. and Richard, S. (2005) Ca^{2+}-dependent reduction of IK1 in rat ventricular cells: a novel paradigm for arrhythmia in heart failure? Cardiovasc. Res. **68**, 204–212
11 Collins, A. and Larson, M. K. (2009) Kir 2.2 inward rectifier potassium channels are inhibited by an endogenous factor in *Xenopus oocytes* independently from the action of a mitochondrial uncoupler. J. Cell. Physiol. **219**, 8–13
12 Vaidyanathan, R., Taffet, S. M., Vikstrom, K. L. and Anumonwo, J. M. (2010) Regulation of cardiac inward rectifier potassium current (IK1) by synapse associated protein-97. J. Biol. Chem. **285**, 28000–28009
13 Loewen, M. E., Wang, Z., Eldstrom, J., Dehghani Zadeh, A., Khurana, A., Steele, D. F. and Fedida, D. (2009) Shared requirement for dynein function and intact microtubule cytoskeleton for normal surface expression of cardiac potassium channels. Am. J. Physiol. Heart Circ. Physiol. **296**, H71–H83
14 Domenighetti, A. A., Boixel, C., Cefai, D., Abriel, H. and Pedrazzini, T. (2007) Chronic angiotensin II stimulation in the heart produces an acquired long QT syndrome associated with IK1 potassium current downregulation. J. Mol. Cell Cardiol. **42**, 63–70
15 Karle, C. A., Zitron, E., Zhang, W., Wendt-Nordahl, G., Kathofer, S., Thomas, D., Gut, B., Scholz, E., Vahl, C. F., Katus, H. A. and Kiehn, J. (2002) Human cardiac inwardly-rectifying K^+ channel $Kir_{2.1b}$ is inhibited by direct protein kinase C-dependent regulation in human isolated cardiomyocytes and in an expression system. Circulation **106**, 1493–1499
16 Kubo, Y., Baldwin, T. J., Jan, Y. N. and Jan, L. Y. (1993) Primary structure and functional expression of a mouse inward rectifier potassium channel. Nature **362**, 127–133
17 Zaritsky, J. J., Redell, J. B., Tempel, B. L. and Schwarz, T. L. (2001) The consequences of disrupting cardiac inwardly rectifying K^+ current (I_{K1}) as revealed by the targeted deletion of the murine Kir2.1 and Kir2.2 genes. J. Physiol. **533**, 697–710
18 Nakamura, T. Y., Artman, M., Rudy, B. and Coetzee, W. A. (1998) Inhibition of rat ventricular IK1 with antisense oligonucleotides targeted to Kir2.1 mRNA. Am. J. Physiol. **274**, H892–H900
19 Zaritsky, J. J., Eckman, D. M., Wellman, G. C., Nelson, M. T. and Schwarz, T. L. (2000) Targeted disruption of Kir2.1 and Kir2.2 genes reveals the essential role of the inwardly rectifying K^+ current in K^+-mediated vasodilation. Circ. Res. **87**, 160–166

20 Jentzsch, C., Leierseder, S., Loyer, X., Flohrschutz, I., Sassi, Y., Hartmann, D., Thum, T., Laggerbauer, B. and Engelhardt, S. (2011) A phenotypic screen to identify hypertrophy-modulating microRNAs in primary cardiomyocytes. J. Mol. Cell. Cardiol. **52**, 13–20

21 Thum, T., Galuppo, P., Wolf, C., Fiedler, J., Kneitz, S., van Laake, L. W., Doevendans, P. A., Mummery, C. L., Borlak, J., Haverich, A. et al. (2007) MicroRNAs in the human heart: a clue to fetal gene reprogramming in heart failure. Circulation **116**, 258–267

22 Tang, Y., Banan, A., Forsyth, C. B., Fields, J. Z., Lau, C. K., Zhang, L. J. and Keshavarzian, A. (2008) Effect of alcohol on miR-212 expression in intestinal epithelial cells and its potential role in alcoholic liver disease. Alcohol Clin. Exp. Res. **32**, 355–364

23 Grimson, A., Farh, K. K., Johnston, W. K., Garrett-Engele, P., Lim, L. P. and Bartel, D. P. (2007) MicroRNA targeting specificity in mammals: determinants beyond seed pairing. Mol. Cell **27**, 91–105

24 John, B., Enright, A. J., Aravin, A., Tuschl, T., Sander, C. and Marks, D. S. (2004) Human MicroRNA targets. PLoS Biol **2**, e363

25 Griffiths-Jones, S., Grocock, R. J., van Dongen, S., Bateman, A. and Enright, A. J. (2006) miRBase: microRNA sequences, targets and gene nomenclature. Nucleic Acids Res. **34**, D140–D144

26 Krek, A., Grun, D., Poy, M. N., Wolf, R., Rosenberg, L., Epstein, E. J., MacMenamin, P., da Piedade, I., Gunsalus, K. C., Stoffel, M. and Rajewsky, N. (2005) Combinatorial microRNA target predictions. Nat. Genet. **37**, 495–500

27 Li, Y. F., Cheng, Y. F., Huang, Y., Conti, M., Wilson, S. P., O'Donnell, J. M. and Zhang, H. T. (2011) Phosphodiesterase-4D knock-out and RNA interference-mediated knock-down enhance memory and increase hippocampal neurogenesis via increased cAMP signaling. J. Neurosci. **31**, 172–183

28 Rinne, A., Littwitz, C., Kienitz, M. C., Gmerek, A., Bosche, L. I., Pott, L. and Bender, K. (2006) Gene silencing in adult rat cardiac myocytes *in vitro* by adenovirus-mediated RNA interference. J. Muscle Res. Cell Motil. **27**, 413–421

29 Chiu, J., March, P. E., Lee, R. and Tillett, D. (2004) Site-directed, Ligase-Independent Mutagenesis (SLIM): a single-tube methodology approaching 100 % efficiency in 4 h. Nucleic Acids Res. **32**, e174

30 Standen, N. B. and Stanfield, P. R. (1978) A potential- and time-dependent blockade of inward rectification in frog skeletal muscle fibres by barium and strontium ions. J. Physiol. **280**, 169–191

31 Preisig Muller, R., Schlichthorl, G., Goerge, T., Heinen, S., Bruggemann, A., Rajan, S., Derst, C., Veh, R. W. and Daut, J. (2002) Heteromerization of Kir2.x potassium channels contributes to the phenotype of Andersen's syndrome. Proc. Natl. Acad. Sci. U.S.A. **99**, 7774–7779

32 Goldoni, D., Zhao, Y., Green, B. D., McDermott, B. J. and Collins, A. (2010) Inward rectifier potassium channels in the HL-1 cardiomyocyte-derived cell line. J. Cell Physiol. **225**, 751–756

33 Seebohm, G., Strutz-Seebohm, N., Ursu, O. N., Preisig-Muller, R., Zuzarte, M., Hill, E. V., Kienitz, M. C., Bendahhou, S., Fauler, M., Tapken, D. et al. (2012) Altered stress stimulation of inward rectifier potassium channels in Andersen–Tawil syndrome. Faseb J. **26**, 513–522

34 Carpenter, A. E., Jones, T. R., Lamprecht, M. R., Clarke, C., Kang, I. H., Friman, O., Guertin, D. A., Chang, J. H., Lindquist, R. A., Moffat, J. et al. (2006) CellProfiler: image analysis software for identifying and quantifying cell phenotypes. Genome Biol. **7**, R100

35 Yang, B., Lin, H., Xiao, J., Lu, Y., Luo, X., Li, B., Zhang, Y., Xu, C., Bai, Y., Wang, H. et al. (2007) The muscle-specific microRNA miR-1 regulates cardiac arrhythmogenic potential by targeting GJA1 and KCNJ2. Nat. Med. **13**, 486–491

36 Sauve, R., Roy, G. and Payet, D. (1983) Single channel K^+ currents from HeLa cells. J. Membr. Biol. **74**, 41–49

37 Klein, H., Garneau, L., Coady, M., Lemay, G., Lapointe, J. Y. and Sauve, R. (1999) Molecular characterization of an inwardly rectifying K^+ channel from HeLa cells. J. Membr. Biol. **167**, 43–52

38 Liu, G. X., Derst, C., Schlichthorl, G., Heinen, S., Seebohm, G., Bruggemann, A., Kummer, W., Veh, R. W., Daut, J. and Preisig-Muller, R. (2001) Comparison of cloned Kir2 channels with native inward rectifier K^+ channels from guinea-pig cardiomyocytes. J. Physiol. **532**, 115–126

39 Zobel, C., Cho, H. C., Nguyen, T. T., Pekhletski, R., Diaz, R. J., Wilson, G. J. and Backx, P. H. (2003) Molecular dissection of the inward rectifier potassium current (IK1) in rabbit cardiomyocytes: evidence for heteromeric co-assembly of Kir2.1 and Kir2.2. J. Physiol. **550**, 365–372

40 Schram, G., Pourrier, M., Wang, Z., White, M. and Nattel, S. (2003) Barium block of Kir2 and human cardiac inward rectifier currents: evidence for subunit-heteromeric contribution to native currents. Cardiovasc. Res. **59**, 328–338

41 Fakler, B., Brandle, U., Glowatzki, E., Weidemann, S., Zenner, H. P. and Ruppersberg, J. P. (1995) Strong voltage-dependent inward rectification of inward rectifier K^+ channels is caused by intracellular spermine. Cell **80**, 149–154

42 Ficker, E., Taglialatela, M., Wible, B. A., Henley, C. M. and Brown, A. M. (1994) Spermine and spermidine as gating molecules for inward rectifier K^+ channels. Science **266**, 1068–1072

43 Lopatin, A. N., Makhina, E. N. and Nichols, C. G. (1994) Potassium channel block by cytoplasmic polyamines as the mechanism of intrinsic rectification. Nature **372**, 366–369

44 Tomaselli, G. F., Beuckelmann, D. J., Calkins, H. G., Berger, R. D., Kessler, P. D., Lawrence, J. H., Kass, D., Feldman, A. M. and Marban, E. (1994) Sudden cardiac death in heart failure. The role of abnormal repolarization. Circulation **90**, 2534–2539

45 Ikeda, S., Kong, S. W., Lu, J., Bisping, E., Zhang, H., Allen, P. D., Golub, T. R., Pieske, B. and Pu, W. T. (2007) Altered microRNA expression in human heart disease. Physiol. Genomics **31**, 367–373

46 Care, A., Catalucci, D., Felicetti, F., Bonci, D., Addario, A., Gallo, P., Bang, M. L., Segnalini, P., Gu, Y., Dalton, N. D. et al. (2007) MicroRNA-133 controls cardiac hypertrophy. Nat. Med. **13**, 613–618

47 Sucharov, C., Bristow, M. R. and Port, J. D. (2008) miRNA expression in the failing human heart: functional correlates. J. Mol. Cell. Cardiol. **45**, 185–192

48 Soltysinska, E., Olesen, S. P., Christ, T., Wettwer, E., Varro, A., Grunnet, M. and Jespersen, T. (2009) Transmural expression of ion channels and transporters in human nondiseased and end-stage failing hearts. Pflugers Arch. **459**, 11–23

49 van Rooij, E., Sutherland, L. B., Liu, N., Williams, A. H., McAnally, J., Gerard, R. D., Richardson, J. A. and Olson, E. N. (2006) A signature pattern of stress-responsive microRNAs that can evoke cardiac hypertrophy and heart failure. Proc. Natl. Acad. Sci. U.S.A. **103**, 18255–18260

50 Chrissobolis, S., Ziogas, J., Chu, Y., Faraci, F. M. and Sobey, C. G. (2000) Role of inwardly rectifying K^+ channels in K^+-induced cerebral vasodilatation *in vivo*. Am. J. Physiol. Heart Circ. Physiol. **279**, H2704–H2712

51 Mayhan, W. G. (1992) Responses of cerebral arterioles during chronic ethanol exposure. Am. J. Physiol. **262**, H787–H791

52 Mayhan, W. G. and Didion, S. P. (1996) Effect of chronic alcohol consumption on responses of cerebral arterioles. Alcohol Clin. Exp. Res. **20**, 538–542

53 Newlin, D. B., Golden, C. J., Quaife, M. and Graber, B. (1982) Effect of alcohol ingestion on regional cerebral blood flow. Int. J. Neurosci. **17**, 145–150

54 MacMahon, S. (1987) Alcohol consumption and hypertension. Hypertension **9**, 111–121

55 Montgomery, R. L., Hullinger, T. G., Semus, H. M., Dickinson, B. A., Seto, A. G., Lynch, J. M., Stack, C., Latimer, P. A., Olson, E. N. and van Rooij, E. (2011) Therapeutic inhibition of miR-208a improves cardiac function and survival during heart failure. Circulation **124**, 1537–1547

56 Suckau, L., Fechner, H., Chemaly, E., Krohn, S., Hadri, L., Kockskamper, J., Westermann, D., Bisping, E., Ly, H., Wang, X. et al. (2009) Long-term cardiac-targeted RNA interference for the treatment of heart failure restores cardiac function and reduces pathological hypertrophy. Circulation **119**, 1241–1252

Received 10 April 2012/3 August 2012; accepted 13 August 2012
Published as BJ Immediate Publication 13 August 2012, doi:10.1042/BJ20120578